Published online 13 April 2015 *Nucleic Acids Research, 2015, Vol. 43, No. 9* ***4463–4476***
doi: 10.1093/nar/gkv304

Linker histone partial phosphorylation: effects on secondary structure and chromatin condensation

Rita Lopez[1], Bettina Sarg[2], Herbert Lindner[2], Salvador Bartolomé[3], Inma Ponte[1], Pedro Suau[1] and Alicia Roque[1,*]

[1]Departamento de Bioquímica y Biología Molecular, Facultad de Biociencias, Universidad Autónoma de Barcelona, 08193, Bellaterra, Barcelona, Spain, [2]Division of Clinical Biochemistry, Biocenter, Innsbruck Medical University, A-6020, Innsbruck, Austria and [3]Laboratorio de Luminiscencia y Espectroscopia de Biomoléculas, Universidad Autónoma de Barcelona, 08193, Bellaterra, Barcelona, Spain

Received October 17, 2014; Revised March 27, 2015; Accepted March 27, 2015

ABSTRACT

Linker histones are involved in chromatin higher-order structure and gene regulation. We have successfully achieved partial phosphorylation of linker histones in chicken erythrocyte soluble chromatin with CDK2, as indicated by HPCE, MALDI-TOF and Tandem MS. We have studied the effects of linker histone partial phosphorylation on secondary structure and chromatin condensation. Infrared spectroscopy analysis showed a gradual increase of β-structure in the phosphorylated samples, concomitant to a decrease in α-helix/turns, with increasing linker histone phosphorylation. This conformational change could act as the first step in the phosphorylation-induced effects on chromatin condensation. A decrease of the sedimentation rate through sucrose gradients of the phosphorylated samples was observed, indicating a global relaxation of the 30-nm fiber following linker histone phosphorylation. Analysis of specific genes, combining nuclease digestion and qPCR, showed that phosphorylated samples were more accessible than unphosphorylated samples, suggesting local chromatin relaxation. Chromatin aggregation was induced by $MgCl_2$ and analyzed by dynamic light scattering (DLS). Phosphorylated chromatin had lower percentages in volume of aggregated molecules and the aggregates had smaller hydrodynamic diameter than unphosphorylated chromatin, indicating that linker histone phosphorylation impaired chromatin aggregation. These findings provide new insights into the effects of linker histone phosphorylation in chromatin condensation.

INTRODUCTION

H1 histones, also known as linker histones, are involved in chromatin higher-order structure and in gene regulation (1). They bind to the outer surface of the nucleosome near the entry/exit point of the linker DNA (2). H1 has multiple isoforms. Somatic mammalian cells contain seven H1 subtypes, designated as H1.1-H1.5, H1.0 and H1.10. An oocyte-specific subtype, H1.8, and three male germ-line-specific subtypes, H1.6, H1.7 and H1.9, have also been identified (3).

The H1 histone complement in chicken erythrocytes is composed of six different subtypes, named H1.01, H1.02, H1.03, H1.10, H1.1L and H1.1R (4). In addition to the H1 subtypes, chicken erythrocytes contain histone H5, a differentiation-specific isoform (5). H5 partially replaces histone H1 in mature erythrocytes, and it is the most abundant subtype in these terminally differentiated cells (6). In immature cells, H5 is phosphorylated, but it becomes progressively dephosphorylated during erythrocyte maturation (7). H5 shows a strong preference for higher-order chromatin structures (8) and binds more tightly to DNA or chromatin than do the H1 subtypes (9,10).

Linker histones have three distinct domains: a short amino-terminal domain (NTD) (20–35 amino acids), a central globular domain (GD) (∼80 amino acids) and a long carboxy-terminal domain (CTD) (∼100 amino acids) (11). The globular domain is extremely conserved, while the terminal domains are highly variable and responsible for family heterogeneity (12). The terminal domains are intrinsically disordered regions that fold upon DNA interaction (13,14). The CTD is involved in chromatin condensation through the binding and neutralization of the charge of the linker DNA (15).

Histone H1 is phosphorylated in a cell-cycle-dependent manner by cyclin-dependent kinases (CDKs) at the consensus sequence (S/T)-P-X-(K/R). The levels of phosphorylation are lowest in G1 and rise during S and G2, becoming maximal at metaphase and sharply decreasing there-

*To whom correspondence should be addressed. Tel: +34 93 5811707; Fax: +34 93 5811264; Email: alicia.roque@uab.es

after (16,17). During interphase, H1 subtypes are present as a mixture of unphosphorylated and low-phosphorylated species, with a proportion of 35–75% of unphosphorylated forms, according to the particular subtype and cell-line and the moment of the cell cycle. H1 is phosphorylated at serine residues in interphase, while threonine residues are additionally phosphorylated in mitosis (18).

We have previously shown that phosphorylation of the CTD by CDKs greatly affects its DNA-bound structure and DNA aggregation capacity (19). The effects of phosphorylation on the secondary structure of the DNA-bound CTD were site-specific and depended on the number of phosphate groups. Partial phosphorylation drastically reduced the DNA aggregation capacity of the CTD, but full phosphorylation restored, to a large extent, the aggregation capacity of the unphosphorylated domain. These results support the involvement of H1 hyperphosphorylation in metaphase chromatin condensation and of H1 partial phosphorylation in interphase chromatin relaxation. However, chromatin is a much more complex substrate than DNA, since the majority of the DNA is wrapped around the nucleosome and not free to interact with histone H1, experiments with chromatin are thus necessary to validate this hypothesis. Previous studies of chromatin reconstituted with unphosphorylated and phosphorylated H1 have shown changes in the thermal denaturation profiles in the presence of phosphorylated H1 (20).

Increasing evidence suggests that histone H1 phosphorylation is involved in chromatin relaxation during the cell-cycle (21–27). H1 phosphorylation during the S-phase has been suggested to be a pre-requisite for DNA replication (22). S172 phosphorylation of H1.5 and H1.2 colocalized at DNA replication and transcription sites (23). H1.4 phosphorylated at S187 is enriched at active 45S pre-ribosomal gene promoters and is rapidly induced at hormone response elements, suggesting that interphase H1 phosphorylation facilitates transcription by RNA polymerases I and II (24). In rat and mouse testes, H1.6 phosphorylation favors the substitution of H1.6 by transition proteins and protamines (25). It has also been shown that partially phosphorylated H5 has reduced affinity for chromatin (26).

The addition of increasing amounts of $MgCl_2$ (0.1–15 mM) to chromatin arrays induces a well-characterized series of hierarchical condensation transitions (28). Chromatin arrays initially fold into a moderately condensed intermediate conformation followed by further condensation into a maximally folded structure whose level of compaction is equivalent to the classic 30-nm diameter fiber. The final condensation transition involves reversible and cooperative oligomerization into a higher-order polymeric species. This phenomenon is also known as chromatin self-association or chromatin aggregation. Partial phosphorylation of linker histones could have an important role in the $MgCl_2$-induced condensation transitions. The elucidation of this role could be of great biological significance, since the regulation of chromatin structure is a key aspect of the control of transcription and other nuclear processes.

We have studied the effects of linker histone partial phosphorylation on secondary structure and chromatin condensation. For that purpose linker histone *ex vivo* phosphorylation with CDK2 in native chromatin, from chicken erythrocytes, was performed. This mixed sequence *in vivo*-based system has the advantage of low levels of both basal endogenous phosphorylation and of non-histone proteins. Infrared spectroscopy analysis of the phosphorylated chromatin samples showed changes in the amide I′, suggesting the induction of β-structure in linker histones upon CDK2 phosphorylation. Thus, the conformational change in linker histones following phosphorylation would be the first step in the molecular mechanism that determines the changes in chromatin condensation. The results of sedimentation through sucrose gradients and of a quantitative nuclease accessibility assay are consistent with the idea that linker histone partial phosphorylation induces chromatin relaxation. Additionally, dynamic light scattering (DLS) measurements showed that linker histone phosphorylation impairs chromatin aggregation induced by $MgCl_2$.

MATERIALS AND METHODS

Preparation of chromatin samples

Short and large chromatin fragments were prepared by micrococcal nuclease digestion of chicken erythrocyte cell nuclei and human embryonic kidney cell nuclei as previously described (29). For details see the Supplementary Materials and Methods.

Ex vivo chromatin phosphorylation

Phosphorylation of linker histones in chicken erythrocyte chromatin was carried out at an equivalent DNA concentration of 2 mg/ml in 50-mM TrisHCl, 10-mM $MgCl_2$, 1-mM ethylene glycol tetraacetic acid (EGTA), 20-mM dithiotreitol, pH 7.5, plus 200-μM adenosine triphosphate (ATP) and 1 μl of a cocktail of protease inhibitors (cOmplete Mini Protease Inhibitor Cocktail Tablets; Roche Applied Biosciences) per 100 μl of reaction. At this point, the mixture was divided into 2. One sample was incubated at 30°C with 1 μl of CDK2-cyclinA kinase (Sigma-Aldrich) per 20 μg of H1, while the other was incubated in the same conditions without kinase. Aliquots were taken after 1 h, 5 h and overnight incubation (on) for further analysis. A radioactive CDK2 phosphorylation assay was also performed (See the Supplementary Materials and Methods and Supplementary Figure S1).

Analysis of linker histone phosphorylation

Linker histones were extracted from the phosphorylated and the initial unphosphorylated chromatin samples, as previously described (30). The incorporation of phosphate groups after *ex vivo* phosphorylation was analyzed by high-performance capillary electrophoresis (HPCE), Matrix Assisted Laser Desorption Ionization Time-of-Flight (MALDI-TOF) mass spectrometry and Tandem Mass Spectrometry (MS/MS) sequencing. Before mass spectrometry analysis the linker histones were fractionated by Reversed-Phase High-Performance Liquid Chromatography (RP-HPLC) and digested with proteolytic enzymes. The detailed protocols are described in the Supplementary Materials and Methods.

Infrared spectroscopy

Chromatin samples were prepared as described in the Supplementary Materials and Methods. Measurements were performed on an FT600 Bio-Rad spectrometer equipped with an Mercury Cadmium Telluride (MCT) detector, using a demountable liquid cell with calcium fluoride windows and 50-μm spacers. Typically, 1000 scans for each background and sample were collected. Spectra were obtained with a nominal resolution of 2 cm^{-1}, at 22°C. The resultant spectra were analyzed with GRAMS 9.0 software (Galactic Corporation). The solvent contribution was eliminated by subtraction of a reference buffer sample. Difference spectra between the phosphorylated and the corresponding unphosphorylated sample were obtained and baseline corrected in the amide I′ region from 1600 cm^{-1} to 1700 cm^{-1} using a linear baseline. Band positions in the difference spectra were confirmed by Fourier deconvolution and assigned as previously described (31). Comparison with the deconvoluted spectrum of water vapor indicates that the protein spectra are free from water vapor artifacts (Supplementary Figure S2A). The estimation of the numbers of linker histone residues involved in the conformational change was made taking into consideration the area percentages of the difference spectra, the linker histone: core histone stoichiometry of the soluble chromatin and the total number of residues of the core histones and linker histones contributing to the amide I′ band.

Sedimentation in sucrose density gradients

Linear sucrose gradients 5–25% in 10-mM Tris pH 8.0, 35-mM NaCl, 1-mM $MgCl_2$ were prepared with a gradient maker (BioRad). To prevent protease activity 1-mM phenylmethylsulfonyl fluoride (PMSF) was added to all solutions. Analytical gradients of phosphorylated and unphosphorylated chromatin samples containing 100–200 μg of DNA were run in a Beckman 55.1 Ti rotor at 40 000 rpm for 1 h at 4°C. After centrifugation and fractionation, histones were digested with proteinase K followed by DNA precipitation. The size of the DNA in the different chromatin fractions was estimated by agarose gel electrophoresis with the software Quantity One (BioRad).

Nuclease accessibility assay

Phosphorylated and unphosphorylated chromatin samples were digested with micrococcal nuclease (1U/200-μg DNA) in the presence of 1.6-mM of divalent cations for 10 min. After digestion, samples were deproteinized overnight with proteinase K at 37°C, and the DNA was purified using a spin column. DNA corresponding to the initial, undigested soluble chromatin was also purified to control the availability of genomic DNA before phosphorylation. Purified DNA was used as a template for the amplification of β-globin and rhodopsin genes by Quantitative Polymerase Chain Reaction (qPCR), following MIQE guidelines, in a C1000^{TM} thermal cycler (BioRad). For details see the Supplementary Materials and Methods and Supplementary Table S1.

Dynamic light scattering

DLS was used to study chromatin aggregation induced by $MgCl_2$ in phosphorylated and unphosphorylated chromatin samples. Measurements were carried out in a ZetaSizer Nano ZS particle analyzer (Malvern Instruments, UK). The light source was a He-Ne laser (633 nm) that uses 5-mW power at the same wavelength. For each measurement, three records were performed. Each record consisted of 14–18 cumulant scans (this parameter is determined automatically to achieve the optimal signal). Samples of soluble and phosphorylated chromatin were diluted with Tris 10-mM pH 7.0, plus 35-mM NaCl, 1-mM $MgCl_2$, to a final concentration of 0.2mg/ml in 1 ml. An initial measurement was made in these conditions. Then, the $MgCl_2$ concentration was increased up to 1.6-mM, and the samples were incubated for 5 min at at 22°C and measured again. For each time, phosphorylated and unphosphorylated chromatin samples were analyzed. The spectra were processed with the high-resolution option of the software to achieve maximal accuracy. Laser diffraction was used to determine the presence of aggregates out of the size range of the DLS (see the Supplementary Materials and Methods).

RESULTS

Characterization of the *ex vivo* phosphorylated chromatin

We have shown that it is possible to *ex vivo* phosphorylate linker histones in chicken erythrocyte chromatin with CDK2. The specificity of the phosphorylation reaction was evaluated with a radioactive CDK2-phosphorylation reaction in the presence of γ-ATP-^{32}P (Supplementary Figure S1). The results of the sodium dodecyl sulphate-polyacrylamide gel electrophoresis (SDS-PAGE) analysis of chromatin total proteins showed that ^{32}P was incorporated into the bands corresponding to linker histones, but not in core histones, indicating that CDK2 specifically phosphorylated linker histones within soluble chromatin. Also, the extent of phosphorylation increased with the time of reaction. A weak band of phosphorylated H3 appeared in all lanes, even when CDK2 was not present, probably due to some residual endogenous kinase activity. SDS-PAGE also confirmed that soluble chromatin contained very low levels of non-histone proteins that were not apparent after Coomassie-Blue staining.

After phosphorylation, linker histones were extracted with perchloric acid and analyzed by HPCE. HPCE allows for the separation of distinct histone subtypes and their post-translational modifications with high sensitivity (32). Two different regions were identified in the HPCE profiles (Figure 1). The first region (I) contained histone H5, its natural variant H5R16Q and their post-translationally modified species (33). In the initial chromatin sample, the intensities of secondary peaks in the profile indicate that the level of basal phosphorylation of chicken erythrocyte chromatin was low. The number and height of the secondary peaks increased considerably in function of the time of phosphorylation, indicating a significant extent of phosphorylation of H5. The second region (II) of the HPCE profile corresponded to the H1 subtypes. In the soluble chromatin sample the six H1 subtypes present in chicken erythrocytes

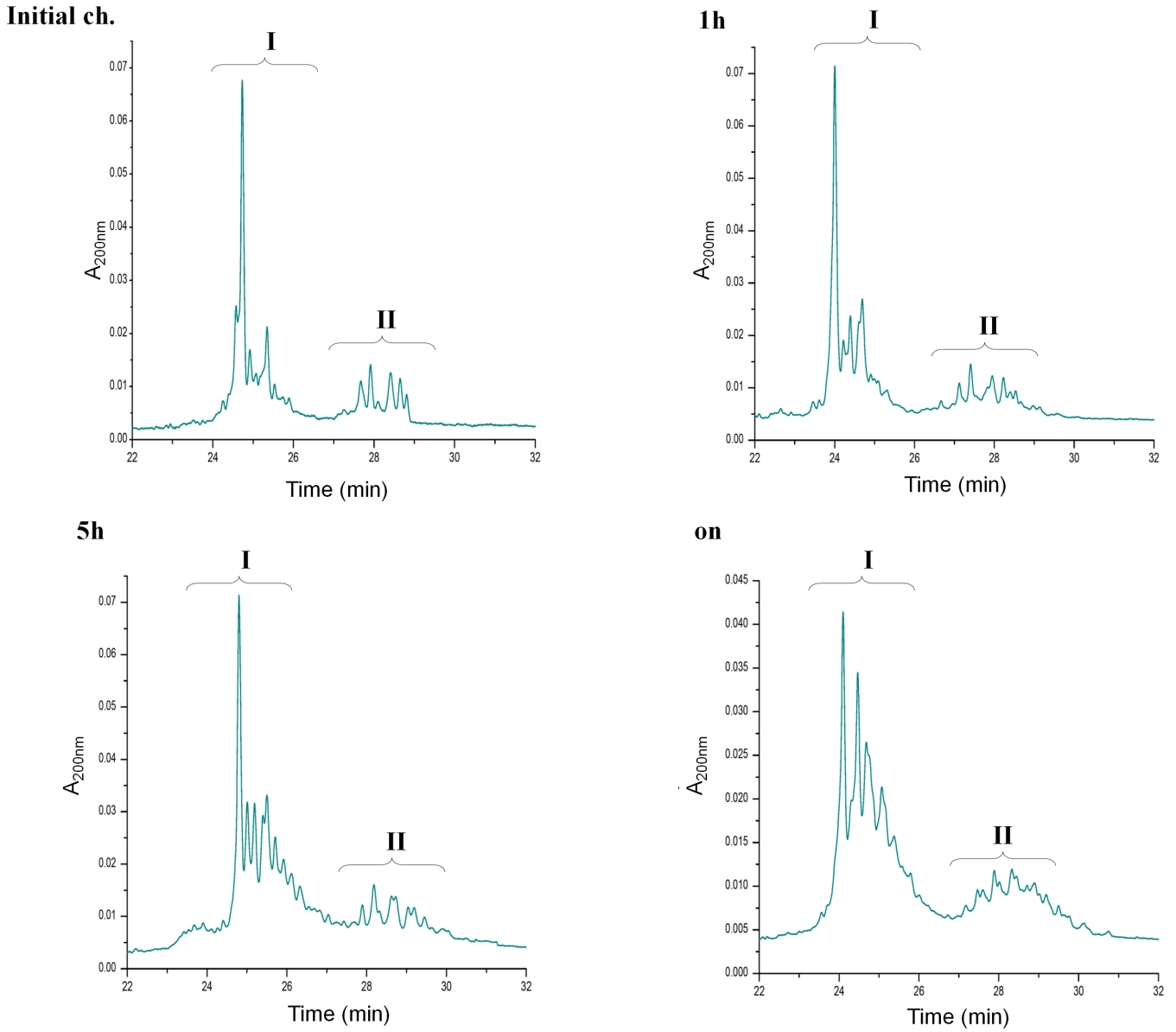

Figure 1. HPCE analysis of the linker histone phosphorylation. HPCE profiles of linker histones extracted from erythrocyte chromatin before phosphorylation (initial ch.) and phosphorylated at 30°C for 1 h, 5 h or overnight (on). Region I corresponds to H5 and its modified species and region II corresponds to H1 subtypes.

could be easily identified. Significant changes in the HPCE profile due to phosphorylation could be seen after 5 h, while after overnight phosphorylation the duplication of the peaks was apparent, suggesting a considerable extent of phosphorylation of H1 subtypes.

After acid extraction, histones H5 and H1 were further separated by RP-HPLC. Partial digestion with α-chymotrypsin of H5 and of the H1 subtypes resulted in two peptides, peptide 1, which comprised the NTD and most of the GD, and peptide 2, which corresponded mainly to the CTD. The resulting peptides were analyzed by MALDI-TOF in order to determine the incorporation of phosphate groups.

In the MALDI-TOF-MS spectra of the H5 samples (Supplementary Figure S3) only one phosphorylated species (peak 4) was detected after overnight phosphorylation, suggesting that this peptide was phosphorylated by CDK2. Although no CDK consensus sequence is present in the NTD of H5, previous studies have reported that S7 is *in vitro* phosphorylated by CDK2 (21). Peptide 2 contains five CDK2 consensus sequences. In the native chromatin sample, a small peak (peak 6) that corresponded to the monophosphorylated species of peptide 2 could be detected. This peak represented ∼12% of peptide 2 in the native chromatin sample, and it further increased up to ∼21, ∼26 and ∼38% after phosphorylation for 1 h, 5 h and overnight, respectively (Supplementary Table S2). The diphosphorylated species of peptide 2 (peak 7) could be detected after 5 h (12%) and overnight phosphorylation (∼17%). In this sample, consid-

ering the mono and diphosphorylated species, 54% of the H5 molecules were phosphorylated.

The H1 fraction contained the six H1 subtypes, so the proteolytic digestion resulted in 12 peptides, which are often post-translationally modified, increasing the number of peptides in the mass spectra. Thus, the systematic identification of all of the peptides in each sample was not possible. In the initial chromatin, all of the identified peptides (Supplementary Table S3) were unphosphorylated, except for some basal phosphorylation in peptide 2 of H1.1R. After overnight phosphorylation, many phosphorylated species could be identified. One monophosphorylated species, which could correspond to the acetylated peptide 1 of H1.03, the only H1 subtype that contains a CDK consensus sequence on the NTD, was detected. Peptide 2 contains three CDK consensus sequences. Mono- or diphosphorylated species of peptide 2 were identified for H1.01, H1.02, H1.1L and H1.1R. A triphosphorylated species, which corresponded to peptide 2 of H1.02, was also identified. These results suggest that H1 subtypes are extensively phosphorylated.

The RP-HPLC-purified H5 and H1 fractions were also enzymatically cleaved with Arg-C and trypsin, respectively, and analyzed by tandem mass spectrometry (LC-ESI-MS/MS), in order to determine if phosphate groups had been incorporated into the CDK consensus sequences (Table 1 and Supplementary Figure S4). Coverage values (Supplementary Table S4) varied between 88 and 38%, with the CTD being the region with less coverage. The limited sequence coverage of the CTD directly affected the identification of the CDK consensus sequences, since most of them were located within this domain. However, CDK motifs in H5, H1.03, H1.1L and H1.1R were identified (Table 1). In native chromatin, all peptides containing CDK consensus sequences, except S155, were unphosphorylated. These peptides became progressively phosphorylated and after overnight phosphorylation their corresponding phosphorylated species could always be identified.

To study the effects of linker histone partial phosphorylation in secondary structure and chromatin condensation we have obtained and phosphorylated preparations of short (10 nucleosomes on average) and long (40 nucleosomes on average) chromatin fragments (Supplementary Figure S5). Chromatin fragments with different length on average were used to analyze possible effects of the fragment size on chromatin aggregation. The chromatin samples were analyzed by transmission electron microscopy. The morphology of the phosphorylated chromatin was quite similar to that of the initial unphosphorylated chromatin. In the conditions assayed containing 1-mM $MgCl_2$, chromatin appeared to be condensed into 30-nm fibers. This fact does not exclude changes in the folding of the 30-nm fiber due to linker histone phosphorylation.

The nucleosomal structure was apparently conserved, as judged by further digestion with micrococcal nuclease (MNase), which gave a characteristic nucleosome ladder (Supplementary Figure S5). Furthermore, there were no changes in the nucleosome repeat length (NRL) of the phosphorylated chromatin with respect to the initial chromatin sample. These results confirmed that phosphorylated linker histones were still dynamically bound to chromatin and, therefore, the phosphorylated samples were suitable for further studies.

Conformational changes of linker histones due to phosphorylation by CDK2

Histone H1 phosphorylation by CDK2 induced a conformational change in the CTD of the protein (19,34; A. Roque, unpublished results). Infrared spectroscopy was used to study changes in the secondary structure following linker histone phosphorylation within chromatin. It is important to note that the changes detected by Fourier transform infrared spectroscopy (FTIR) will be related to linker histone phosphorylation, since linker histones are the only substrates of CDK2 in erythrocyte chromatin (Supplementary Figure S1).

FTIR measurements of the chromatin samples were performed and the spectra of the amide I′ region (1600–1700 cm^{-1}) of each sample were analyzed. This region, mostly composed of the stretching vibration of the polypeptide backbone carbonyl, is an indicator of secondary structure (31,35). With increasing phosphorylation time, a shift of the maximum of the spectra to lower wavelengths, with respect to the initial chromatin sample, was observed in the phosphorylated samples. In the short chromatin fragments, the maximum shifted from 1654 cm^{-1} to 1651 cm^{-1} (Figure 2A), while in the long chromatin fragments the shift was from 1656 cm^{-1} to 1652 cm^{-1} (Supplementary Figure S6A).

The amide I′ band of the chicken erythrocyte chromatin samples contains contributions of core histones, linker histones and DNA. To further analyze the changes due to linker histone partial phosphorylation, a difference spectrum between each phosphorylated sample with the corresponding unphosphorylated sample was obtained (Figure 2B and Supplementary Figure S6B). The difference spectra showed a positive contribution in the 1600–1640 cm^{-1} region with three distinct peaks at 1616–1618 cm^{-1}, 1623–1625 cm^{-1} and 1632–1634 cm^{-1}, all of them corresponding to β-structure (36). At the same time, a negative contribution was observed in the 1640–1680 cm^{-1} region, with a single and broad peak centered at 1657–1658 cm^{-1}, a region that has been assigned to either α-helix or turns (36). The position of each component assigned to β-structure was confirmed by Fourier deconvolution of the difference spectra (Supplementary Figure S2B and C). Deconvolution of the negative region of the difference spectra (1640–1680 cm^{-1}) resulted in three distinct components, the most intense centered at 1655–1657 cm^{-1} corresponding to α-helix/turns. The other two components were centered at 1666–1667 cm^{-1} and 1675–1678 cm^{-1}, positions usually assigned to turns.

The area of the positive region from 1600 cm^{-1} to 1640 cm^{-1} and that of the negative region from 1640 cm^{-1} to 1680 cm^{-1} were similar and indicated the percentage of the total amide I′ region that changes its secondary structure upon phosphorylation (Figure 2C and Supplementary Figure S6C). The area values increased with time of phosphorylation from ∼2% after 1 h of phosphorylation up to ∼6–7% in the overnight sample. These results indicated that phosphorylation induced a conformational change in linker histones characterized by an increase in β-structure at

Table 1. Phosphorylated peptides of the chicken linker histones identified by MS/MS

Protein	Phosphorylated residue	Position	Peptide sequence	Soluble chromatin	Phosphorylated chromatin		
					1 h	5 h	Overnight
H5	**S148**	143–150	KKSRApSPK		√	√	√
H1.03	**T16**	1–19	AETAPVAAPDVAAAPpTPAK		√	√	√
H1.03, H1.1L, H1.1R	**S155**	148–159 (H1.1L)	KAVAVKKpSPK	√[a]			√
H1.03	**S191**	186–194	AVAVKpSPAK			√	√
H1.1R, H1.1L	**S192**	186–197 (H1.1L)	KAVAAacKpSPAKAK		√	√	√

The bold letters correspond to phosphorylated residues of the CDK consensus sequences. √: phosphorylated peptide detected; ac: acetylation; p: phosphorylation.
[a]This peptide was found phosphorylated in very small proportion in the initial chromatin samples (see that the phosphorylated peptide was undetected after 1 h or 5 h of phosphorylation), but became readily detected after overnight phosphorylation.

the expense of α-helix/turns. Taking into consideration the linker histone:core histone stoichiometry, the latter values indicate that after overnight phosphorylation ∼70 residues of each linker histone are involved in the conformational change.

Linker histone partial phosphorylation promotes chromatin relaxation

We have studied the sedimentation profile of unphosphorylated and phosphorylated chromatin using linear sucrose gradients. This technique allows the separation of chromatin fragments by their differential sedimentation rate which depends on the mass, density and shape (37). An additional advantage of the use of the sucrose gradients is that chromatin fractions are free of soluble components.

The results of the separation of the phosphorylated and unphosphorylated chromatin through sucrose gradients in 35-mM NaCl and 1-mM $MgCl_2$ are shown in Figure 3. In these conditions the chromatin fragments are mostly folded in the 30-nm fiber but not aggregated. Partial linker histone phosphorylation decreased the sedimentation rate of the chromatin fragments. Equivalent fractions of the same density contained chromatin fragments of higher molecular weight when chromatin was phosphorylated overnight. Differences of ∼200 bp were detected in fraction 4 and they became larger as the length of the chromatin fragments increased, reaching ∼2500 bp in fraction 17.

A similar effect was observed with chromatin fragments isolated from human embryonic kidney cells, which contained ∼59% of partially phosphorylated H1 (Supplementary Figure S7). In this cellular type differences of more than 500 bp were detected also in fraction 4. The differences increased with the length of the chromatin fragments, reaching more than 4000 bp. Short DNA fragments were found throughout the fractions, probably due to the high concentration of the chromatin loaded on the gradient, which could cause a drag effect on the small fragments by the larger ones. These results showed that the changes described above were not specific of chicken erythrocyte chromatin, but common to any CDK2-phosphorylated chromatin. Moreover, the shift in the sedimentation rate observed upon phosphorylation was not a consequence of the loss or degradation of the linker histone component as shown in Figure 3D and Supplementary Figure S7F. In summary, the sedimentation analysis results indicate that linker histone partial phosphorylation induces global relaxation of the chromatin fiber.

Linker histone partial phosphorylation increases chromatin accessibility to MNase

We have examined the chromatin accessibility in two specific genes in phosphorylated and unphosphorylated chromatin samples, combining micrococcal nuclease digestion and qPCR. In this assay, a micrococcal nuclease digestion was performed after the induction of chromatin aggregation with 1.6-mM of divalent cations. After digestion, two specific gene fragments were quantified by qPCR. The extent of digestion of each sample determined the quantity of DNA suitable for PCR amplification and, thus, the Ct (threshold cycle) value. ΔCt, taking the initial chromatin sample as a reference, would be higher in the samples with a more extensive digestion and, therefore, more accessible to nuclease. The fold decrements in template availability, calculated as $2^{\Delta Ct}$, were used as a measure of chromatin accessibility. Two amplicons were quantified; a fragment of the β-globin gene, which is potentially active in mature erythrocytes, and a fragment of the rhodopsin gene, which is an epigenetically silenced gene.

The results of the amplification of β-globin and rhodopsin genes in samples of short and long chromatin fragments are summarized in Supplementary Table S5. The Ct values for the phosphorylated chromatin were always higher than were those of the corresponding unphosphorylated sample, indicating a greater accessibility to MNase. This was true for short and long chromatin fragments. For short chromatin fragments, the template DNA for the β-globin gene in the phosphorylated samples decreased ∼8-fold, while it decreased less than 4-fold in the unphosphorylated samples. For the rhodopsin gene, the decrement in the phosphorylated samples was ∼12-fold, while, for the unphosphorylated samples, it was less than 6-fold (Figure 4).

For long chromatin fragments, the ΔCt values were lower than those in the short chromatin fragments due to the fact that both chromatin samples were digested in the same conditions (same amount of nuclease and equal time of digestion) (Supplementary Table S5 and Figure 4). There-

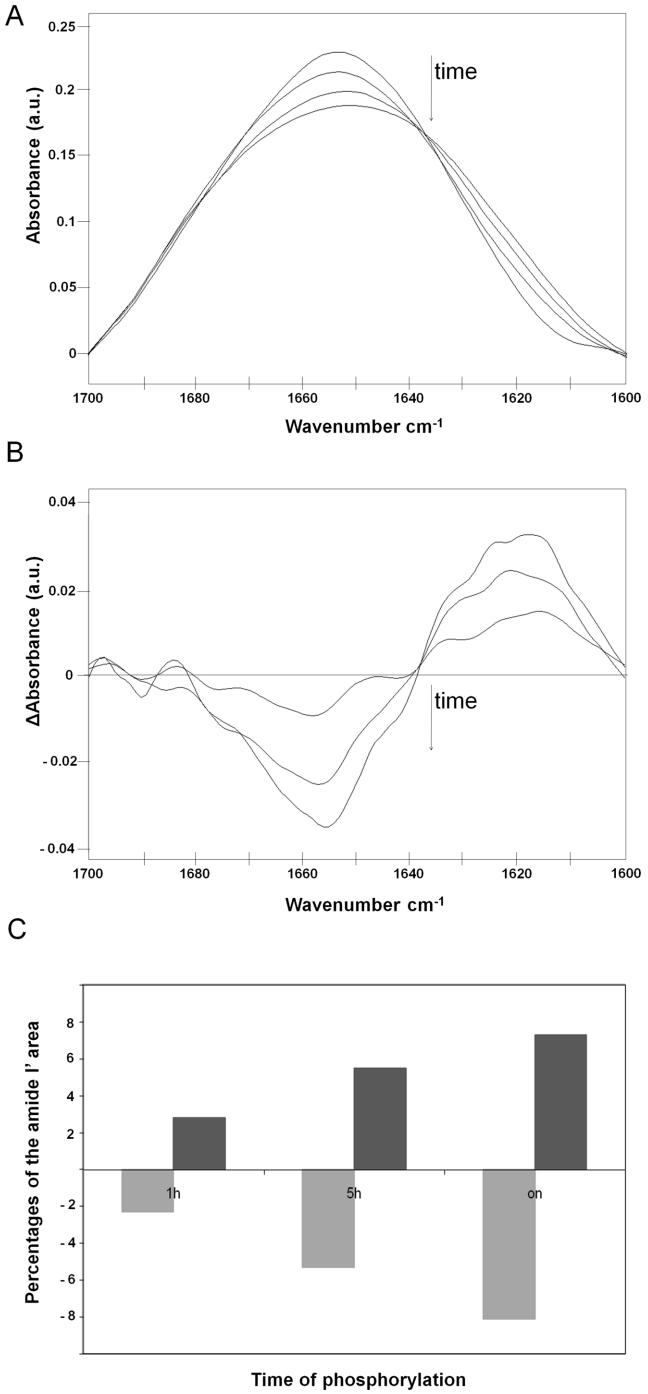

Figure 2. FTIR analysis of the phosphorylated short chromatin fragments. (**A**) Spectra in the amide I′ region (1600–1700 cm^{-1}) of the initial chromatin and of the phosphorylated samples at different times (1h, 5h and overnight, on). (**B**) Difference spectra between the unphosphorylated chromatin and the phosphorylated samples. (**C**) Percentages of the total amide I′ area of the difference spectra assigned to β-structure (dark gray) and to α-helix/turns (light gray). Arrows in panels A and B indicate the increase in the time of phosphorylation.

fore, in longer chromatin fragments the decrements in template DNA were lower. Taken together, the results show that partially phosphorylated chromatin samples displayed higher chromatin accessibility than did the unphosphorylated samples.

Linker histone partial phosphorylation impairs chromatin aggregation induced by $MgCl_2$

DLS has been used to study the effects of partial H1/H5 phosphorylation on the Mg^{2+}-dependent aggregation of chicken erythrocyte chromatin fragments. A series of measurements in buffers of different composition were performed (Supplementary Figure S8A). Samples could not be measured without salt (10-mM Tris buffer). This likely reflected the flexibility of decondensed chromatin fragments in these conditions. Measurements were already feasible in 10-mM NaCl, where a single peak was observed, with a hydrodynamic diameter of ∼88 nm. In 35-mM NaCl, the hydrodynamic diameter fell to ∼82 nm. The same value was observed at 50-mM NaCl. The decrease of the hydrodynamic diameter was likely determined by the combined effects of some degree of intramolecular chromatin compaction in 35-mM NaCl and to the suppression of the double layer of ions around the particle (Debye length) upon increased conductivity.

Measurements were thus performed in 35-mM NaCl plus a specified concentration of Mg^{2+} ions. The addition of 1-mM $MgCl_2$ led to extensive intramolecular compaction of the chromatin fiber, as indicated by a drastic decrease of the hydrodynamic diameter down to ∼50 nm (Supplementary Figure S8B). A further increase up to 1.6-mM of the concentration of $MgCl_2$ led to the appearance of a second peak of aggregated chromatin fragments (≥200 nm) with a much higher hydrodynamic diameter. At 1.6-mM $MgCl_2$, the first peak remained approximately at the same position as in 1-mM $MgCl_2$, indicating that in 1-mM $MgCl_2$ intramolecular fiber compaction, inside the sensitivity of DLS measurements, was already maximal (Supplementary Figure S8C).

In order to observe the effects of phosphorylation on chromatin aggregation, samples were incubated in the presence of CDK2 for 1 h, 5 h and overnight at 30°C. Incubation at 30°C induced, by itself, the aggregation of part of the sample in a time-dependent manner when chromatin was in the presence of 1.6-mM $MgCl_2$ (Supplementary Figure S8C). However, no significant aggregation was observed in 1-mM $MgCl_2$ upon incubation at 30°C (Supplementary Figure S8B). Chromatin aggregation was thus dependent at the same time on the presence of a critical concentration of Mg^{2+} ions and the temperature and time of incubation. The effects of phosphorylation on chromatin aggregation were, therefore, evaluated in comparison with the degree of aggregation of samples incubated during the same time periods at 30°C, but without kinase (Figures 5 and 6 and Supplementary Table S6).

Preparations of short and long chromatin fragments were analyzed (Figures 5 and 6 and Supplementary Figure S8). Figure 4 shows the DLS scans of phosphorylated and unphosphorylated short chromatin fragments in 1.6-mM $MgCl_2$. In these conditions, a bimodal distribution was observed. The hydrodynamic diameter of the first peak

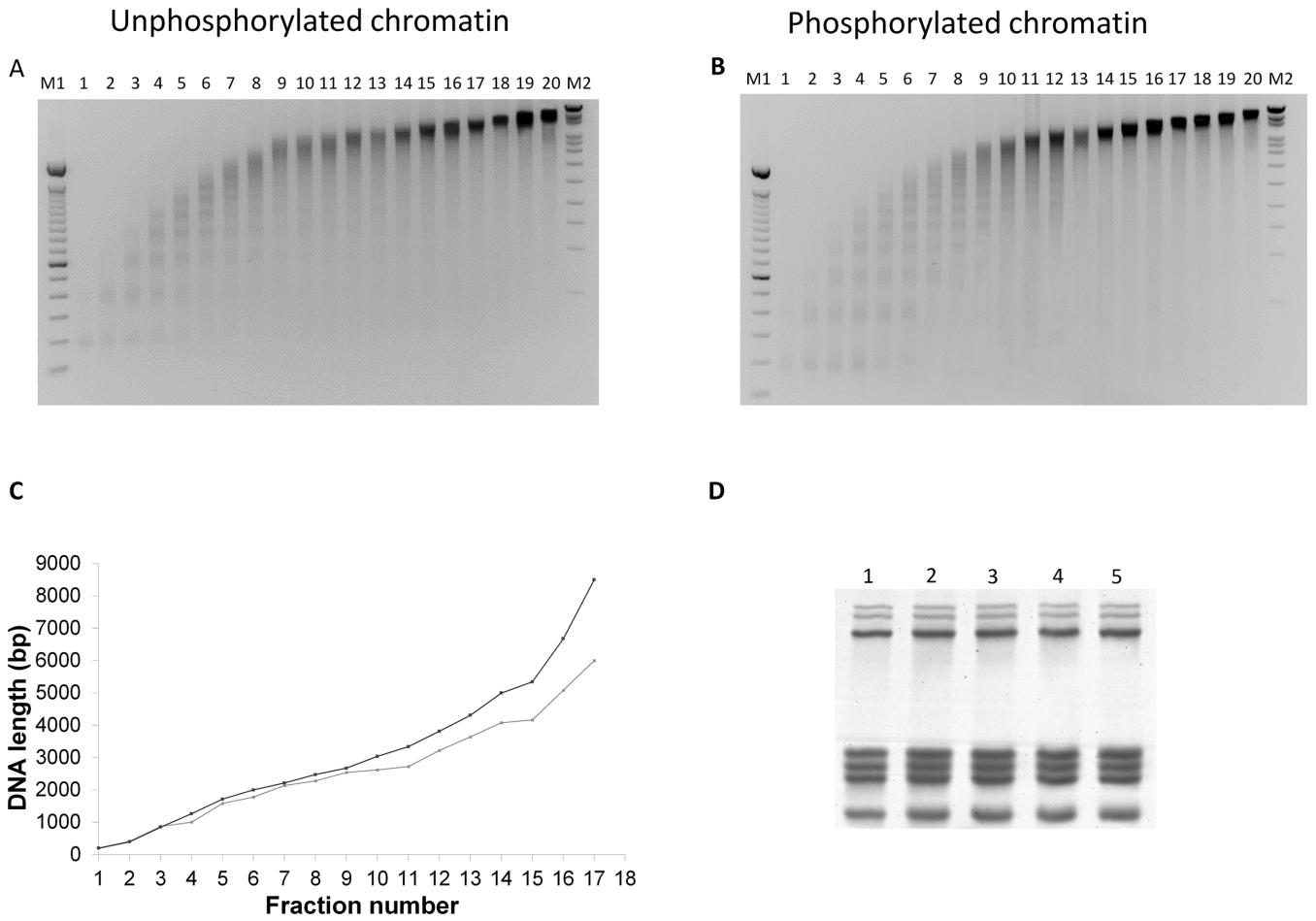

Figure 3. Sedimentation through sucrose linear gradients of the chromatin samples. 1.5% agarose gel electrophoresis of the DNA extracted from the gradient fractions corresponding to the unphosphorylated (**A**) and phosphorylated overnight (**B**) chromatin samples. The DNA present in the chromatin samples was precipitated after treatment with proteinase K. M1: 100-bp DNA ladder (Invitrogen); M2: DNA molecular weight marker IV (Roche). (**C**) Plot with the estimated sizes of the DNA in the phosphorylated (dark gray) and unphosphorylated (light gray) samples. (**D**) 15% SDS-PAGE of the proteins present in the chromatin samples: lane 1, initial chromatin; lanes 2, 3, fractions 14 and 15 of the unphosphorylated chromatin gradient; lanes 4, 5, fractions 14 and 15 of the phosphorylated chromatin gradient. The proteins in the samples from the gradients were previously precipitated with TCA 20%.

was ∼50 nm, both in unphosphorylated and phosphorylated chromatin. The value was similar to that observed in 1-mM $MgCl_2$ and corresponded to non-aggregated chromatin. The hydrodynamic diameter of the aggregation peak increased with incubation time in unphosphorylated chromatin. Values of 200.1, 194.6 and 304.5 nm were observed after 1 h, 5 h and overnight incubation at 30°C. Phosphorylation decreased the size of the aggregation peaks, except for the shorter time of phosphorylation (1 h). In the presence of kinase, values of hydrodynamic diameter of 200.1, 171.9 and 235.9 nm were observed after 1 h, 5 h and overnight incubation, respectively (Figure 5 and Supplementary Table S6).

The intensity distribution was converted into a volume distribution using the Mie theory. Volume distribution gives a more realistic view of the importance of the second peak than does the intensity distribution. In our case, the transformation was needed, since the effects of phosphorylation were not only on the size of the aggregates but also on the fraction of the sample volume (%) represented by the aggregates. With short chromatin fragments, phosphorylation reduced the volume fraction of aggregates by 2–7-fold, depending on the time of incubation. The effect of phosphorylation was thus both on the size and the amount of the aggregates. The volume size distribution shows that aggregates are present in low concentrations, with values that varied between 2.2 and 16.8% (Supplementary Table S6).

In long chromatin fragments, the hydrodynamic diameter of the first peak of non-aggregated molecules was slightly higher, 54 versus 50 nm, than that observed with shorter chromatin fragments (Figure 6 and Supplementary Table S6). Considering that in the presence of 1.6-mM $MgCl_2$ the chromatin fiber is fully condensed, with packing ratios of six or higher, a larger difference was not expected. The hydrodynamic diameters of the aggregation peaks were, instead, much larger than in shorter chromatin fragments. The volume fraction of the aggregates varied between 9.4 and 35.6% in long chromatin fragments. It was thus much larger than it was in short chromatin fragments. As with short chromatin fragments, the volume fraction (%) represented by the aggregates decreased in the phosphorylated samples in relation to the controls.

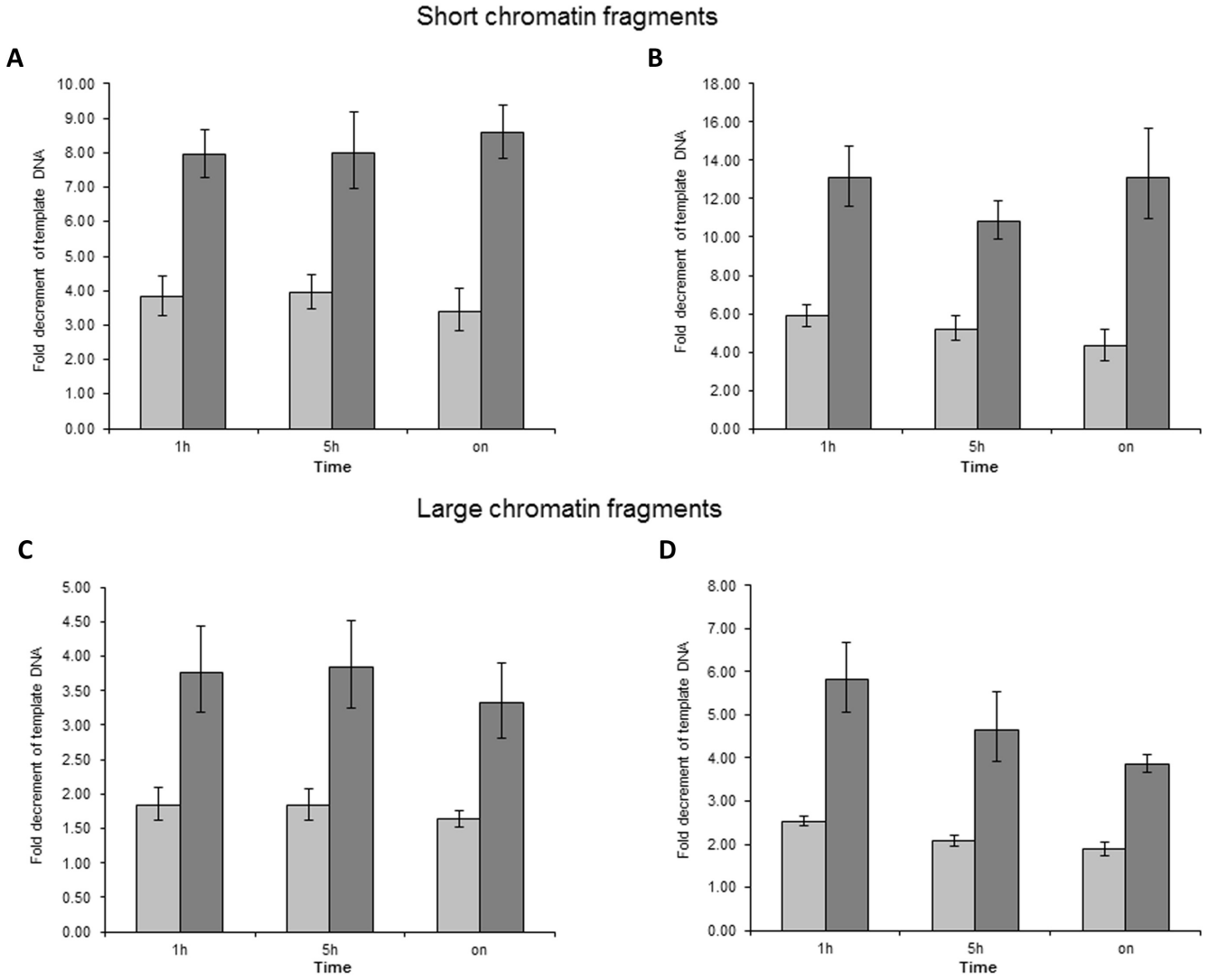

Figure 4. Fold decrements of template DNA of the β-globin and rhodopsin genes after MNase digestion of chromatin samples quantified by qPCR. Dark gray, phosphorylated samples. Light gray, unphosphorylated samples. (**A, C**) Results for the β-globin gene. (**B, D**) Results for the rhodopsin gene. Fold decrements were calculated as $2^{\Delta Ct}$, using the Ct value of the initial undigested chromatin sample as reference for each gene. Error bars correspond to the interval $2^{\Delta Ct \pm SD}$.

After 1 h of incubation without kinase, the second peak had a hydrodynamic diameter of 482 nm, whereas in the presence of kinase it had 255.9 nm. After 5 h of incubation, the corresponding values were 795.5 and 344 nm. After overnight incubation a third peak was observed with hydrodynamic diameter values of 1375 and 721 nm for the unphosphorylated and phosphorylated samples, respectively (Figures 5 and 6 and Supplementary Table S6). Long incubation times thus favored the formation of larger aggregates. Overall, phosphorylation of large chromatin fragments decreased the hydrodynamic diameter of the aggregates by about half. These results clearly indicate that partial phosphorylation significantly decreases both the size and the relative amount of the aggregates formed at 30°C in the presence of magnesium ions.

DISCUSSION

In interphase, partial histone H1 phosphorylation is supposed to be involved in chromatin relaxation (21–27). We have previously shown that H1 partial phosphorylation by CDK2 decreases the DNA aggregation capacity of the CTD of histone H1 and also induces structural changes in the protein (19). These results led to the question of the effects on secondary structure and chromatin condensation of linker histone partial phosphorylation in a chromatin context.

To address this question we phosphorylated chicken erythrocyte chromatin. The soluble chicken erythrocyte chromatin fraction is particularly useful, since it has a very low content of non-histone proteins and low levels of basal phosphorylation. The results indicate that linker histones were partially phosphorylated. A progression of phosphorylation over time was observed. MALDI-TOF relative

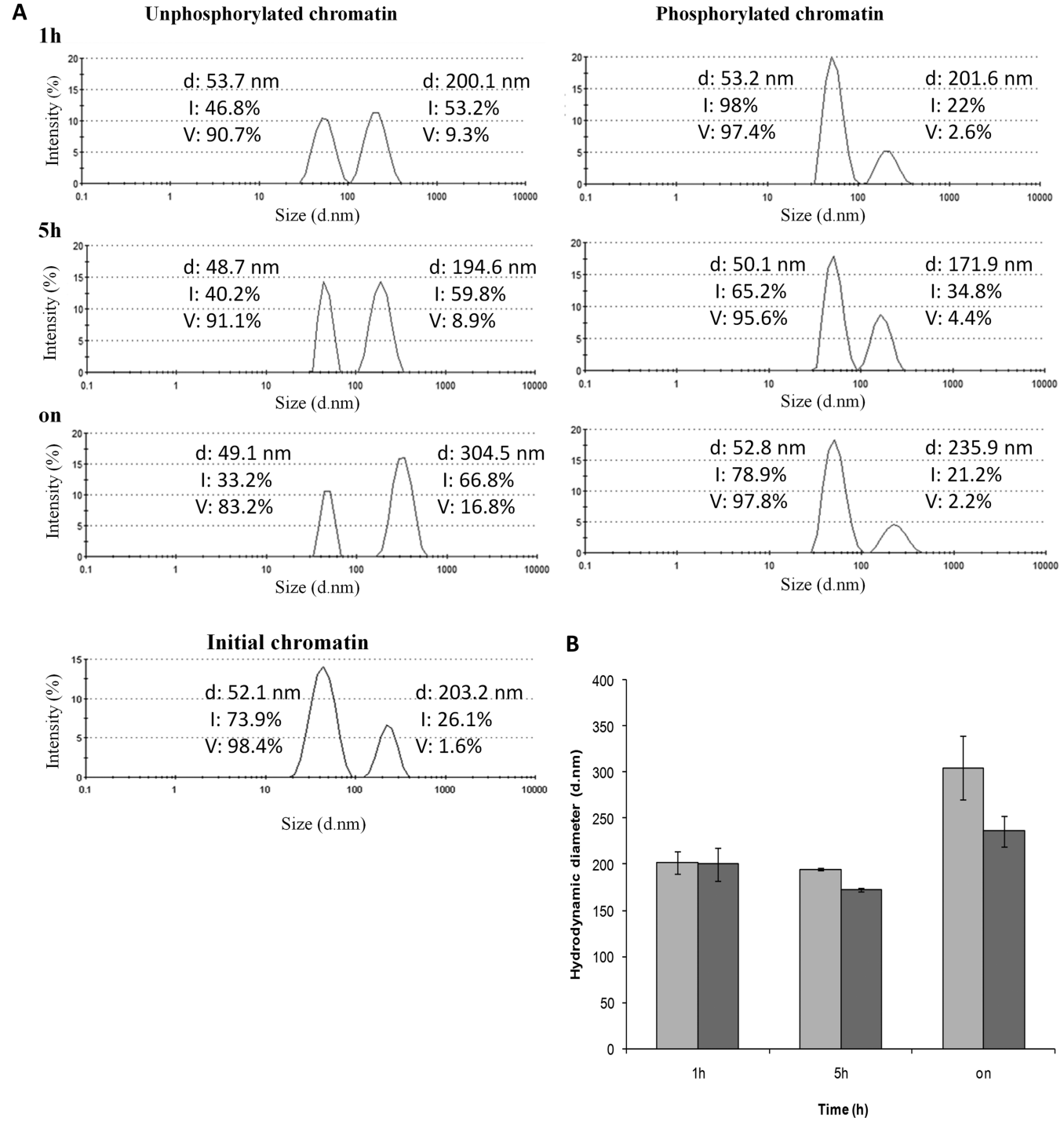

Figure 5. DLS analysis of short chromatin fragments. Panel (**A**) corresponds to DLS size distributions of short chromatin fragments in 1.6-mM $MgCl_2$. The left panel corresponds to unphosphorylated chromatin and the right panel corresponds to phosphorylated chromatin. Chromatin samples were at 0.2 mg/ml in Tris 10-mM, NaCl 35-mM plus 1.6-mM $MgCl_2$, and incubated at 30°C for 1 h, 5 h or overnight (on). The DLS spectrum at the bottom of the left panel corresponds to the initial chromatin sample in 1.6-mM $MgCl_2$. For each peak the hydrodynamic diameter (*d*), percentage of intensity (*I*) and percentage of the volume fraction (*V*) are shown. (**B**) Plot of hydrodynamic diameter values of the more aggregated peak in the DLS scan of each sample. Light gray, unphosphorylated chromatin. Dark gray, phosphorylated chromatin. Error bars correspond to the standard deviation.

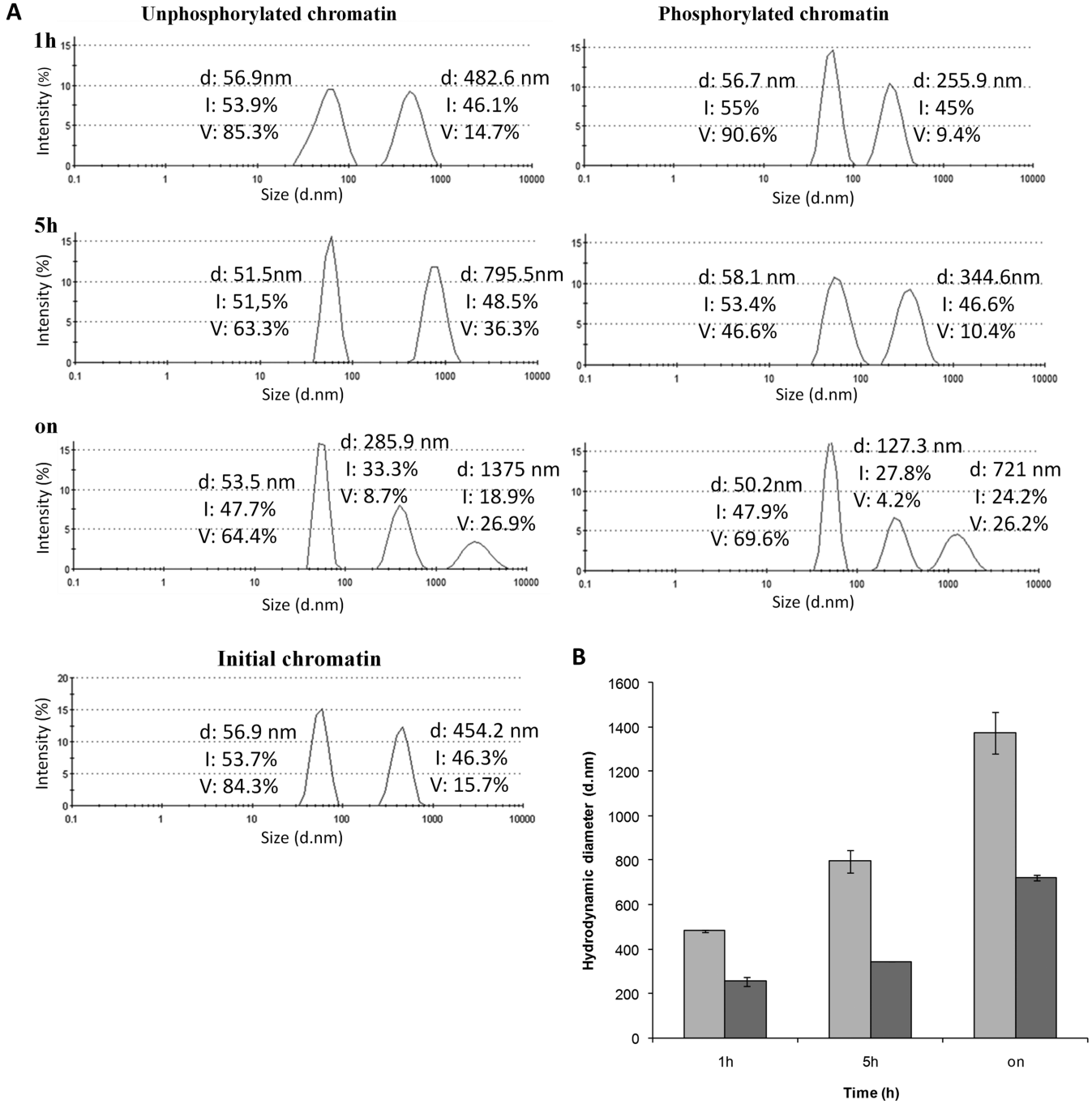

Figure 6. DLS analysis of large chromatin fragments. Panel (**A**) corresponds to DLS size distributions of large chromatin fragments in 1.6-mM $MgCl_2$. The left panel corresponds to unphosphorylated chromatin and the right panel corresponds to phosphorylated chromatin. Chromatin samples were at 0.2 mg/ml in Tris 10-mM, NaCl 35-mM plus 1.6-mM $MgCl_2$, and incubated at 30°C for 1 h, 5 h or overnight (on). The DLS spectrum at the bottom of the left panel corresponds to the initial chromatin sample in 1.6-mM $MgCl_2$. For each peak the hydrodynamic diameter (*d*), percentage of intensity (*I*) and percentage of the volume fraction (*V*) are shown. (**B**) Plot of hydrodynamic diameter values of the more aggregated peak in the DLS scan of each sample. Light gray, unphosphorylated chromatin. Dark gray, phosphorylated chromatin. Error bars correspond to the standard deviation.

quantification showed that after overnight phosphorylation 54% of H5 CTD was phosphorylated. This value is particularly relevant, since H5 represents 70% of the linker histone complement of chicken erythrocytes and can be used as a reference of the extent of phosphorylation.

The structural effects of linker histone phosphorylation in chromatin were studied by FTIR. The results showed a shift in the maximum of the spectra of the amide I′ (1600–1700 cm^{-1}) to lower wavelengths with increasing phosphorylation time. Further analysis of the difference spectra between the phosphorylated and unphosphorylated samples revealed that the secondary structure change consisted in an increase in the β-structure content at the expense of α-helix/turns. There was also an increase in the percentages of the amide I′ involved in the secondary structure changes, concomitant to the increase in linker histone phosphorylation, suggesting the direct relationship between the two events.

FTIR analyses are in agreement with studies performed with whole H1.0, H1.2 and H1.4 (A.Roque, unpublished results) where partial phosphorylation of the CTD was capable of inducing a significant increase in the β-structure content of the whole protein when bound to DNA, presumably as a result of the folding of the CTD. The FTIR results indicate that the changes in the secondary structure following CDK2 phosphorylation also take place within chromatin, highlighting their biological importance (19,34).

A direct consequence of the induction of β-structure could be a less efficient neutralization of the linker DNA, which would increase the exchange rate of linker histones and, thus, favor local chromatin relaxation (36). Several studies indicate that partial linker histone phosphorylation is necessary for replication, transcription and other cellular processes (22–25). Traditionally, the effects of phosphorylation have been explained by a decrease of the positive net charge associated with the incorporation of the phosphate groups (20). However, a more significant contribution to the decrease of the CTD electrostatic potential could arise from the folding in β-sheet conformation, since 70% of the Lys residues of the CTD are in doublets that would project in opposite directions in the sheet-like structure (38). This arrangement would decrease the level of charge neutralization. It has also been shown that the C-terminal domain is the primary determinant of linker histone binding to chromatin *in vivo* and is involved in the secondary and tertiary folding of nucleosomal arrays (39–41), therefore phosphorylation-induced changes within this domain could have great effects on chromatin condensation. Model calculations support the role of the CTD in salt-dependent chromatin condensation and also suggest that phosphorylation should enhance more open chromatin structures and nucleosome accessibility, thus favoring transcription (42).

Global and local changes in chromatin relaxation upon linker histone phosphorylation were also examined. Sedimentation through linear sucrose gradients have been widely used to analyze structural changes in chromatin (43–46). Our results showed global changes in chromatin compactness following phosphorylation characterized by an increase in the molecular weight of the fragments of the phosphorylated samples in equivalent fractions with respect to the unphosphorylated samples, indicating a global relaxation of the chromatin fibers. These effects increased with the length of the chromatin fragment and it is not a consequence of a loss or degradation of the linker histone component.

The analysis of chromatin samples from human embryonic kidney cells showed even greater changes in the sedimentation rate upon phosphorylation, probably because the percentage of partially phosphorylated linker histones was slightly higher than in chicken erythrocyte chromatin. These results indicate that the effects of linker histone phosphorylation are not restricted to chicken erythrocyte chromatin and emphasize their physiological relevance.

Chromatin accessibility to MNase was quantified by qPCR, which allowed to measure local changes in chromatin relaxation. Chicken erythrocyte chromatin is highly compact and almost transcriptionally inactive. To ascertain that linker histone phosphorylation has the same effects on potentially different chromatin regions, we selected the β-globin gene, one of the potentially active genes in mature erythrocytes, and the rhodopsin gene, which is expressed only in retina, and thus, epigenetically silenced (47).

Phosphorylated samples had higher Ct values than did the unphosphorylated samples, which resulted in higher fold decrements in template availability following MNase digestion. The same trend was observed in short and large chromatin fragments in both of the tested genes, confirming that phosphorylation has the same effects on genes with a different genomic context. The fold decrements in template availability indicate that chromatin in the phosphorylated samples was about twice more accessible to MNase than it was in the unphosphorylated samples, suggesting local chromatin relaxation. Taken together, the results of the sedimentation analysis and of the chromatin accessibility assay indicate that linker histone phosphorylation favors chromatin relaxation (20,27,48,49).

The role of linker histones is to stabilize the formation of the 30-nm fiber, as well as the formation of higher order polymeric structures (50,51). The addition of increasing amounts of $MgCl_2$ induces chromatin compaction into the 30-nm fiber, followed by cooperative oligomerization (28). DLS results showed that the addition of 1-mM $MgCl_2$ caused a decrease in the chromatin hydrodynamic diameter in both phosphorylated and unphosphorylated samples, suggesting chromatin condensation in the 30-nm fiber. These results were confirmed by electron microscopy.

At 1.6-mM $MgCl_2$, the peak of condensed chromatin coexisted with a peak of aggregated chromatin, which was still within DLS range. The results showed that phosphorylated samples had aggregates with lower hydrodynamic diameters. Also, the volume fraction corresponding to the aggregated molecules in the phosphorylated samples was lower. These results indicate that the extent of chromatin aggregation was lower when linker histones were partially phosphorylated and corroborate, in a biological context, the conclusions of previous studies with naked DNA (19).

Our results show that linker histone partial phosphorylation impaired chromatin aggregation and, thus, the formation of higher-order polymeric structures. This finding could be of great biological significance, since the regulation of chromatin tertiary structures through linker histone phosphorylation could contribute to regulate gene expres-

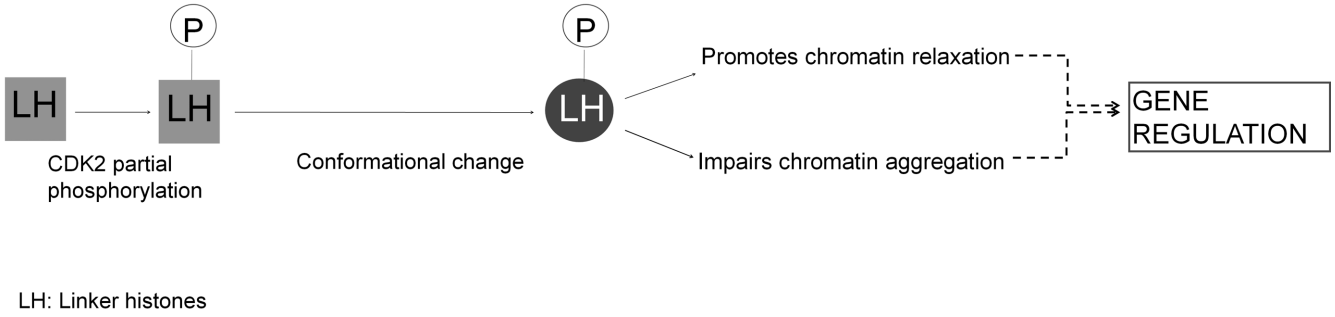

Figure 7. Schematic representation of the effects of linker histone partial phosphorylation.

sion. It has been proposed that phosphorylation of histone H1 could act as a first-step mechanism for inducing chromatin remodeling, enabling access of factors for gene activation, DNA replication and repair (23).

Linker histones bind dynamically to chromatin. The exchange rate could be determined by the H1 affinity for DNA and, therefore, modulated by phosphorylation. Partial phosphorylation moderately decreases the affinity of H1 and its CTD for DNA (19, unpublished results). Phosphorylated linker histones can still bind to chromatin, though with lower affinity than the unphosphorylated species. This fact would explain the increased mobility of the phosphorylated species (48,49), their displacement by other nuclear proteins (1,52) and their general role in promoting chromatin relaxation (20,26). Under our conditions we had no significant amounts of non-histone proteins and the majority of the partially phosphorylated linker histones, which represented about one half of the total linker histones, remained bound to chromatin, as shown by the 30-nm chromatin fibers observed by Transmission Electron Microscopy (TEM) and DLS, the constant length of the NRL and the proportion of linker histones present in the individual fractions after the sucrose gradients.

The effects linker histone partial phosphorylation on secondary structure and chromatin condensation are summarized in Figure 7. We provide evidence, for the first time, at chromatin level, that the effects of partial phosphorylation are determined by the induction of β-structure in the CTD of linker histones, and are not a simple effect of the net charge. We have shown that linker histone partial phosphorylation induced chromatin relaxation, which would enable access of nuclear factors or complexes to certain genes. Linker histone partial phosphorylation also impaired chromatin aggregation and thus the formation of higher-order chromatin structures. Therefore, partial phosphorylation of linker histones could have an important role in gene expression.

SUPPLEMENTARY DATA

Supplementary Data are available at NAR Online.

ACKNOWLEDGEMENTS

We thank the Laboratorio de Luminiscencia y Espectroscopia de Biomolècules for the use of the facilities to perform the infrared spectroscopy measurements and the qPCR experiments. We also thank the Servei de Granges i Camps experimentals of the UAB for providing the chicken blood and J. Lorenzo for providing the HEK cell culture.

FUNDING

The Ministerio de Ciencia e Innovación [BFU2008-00460]. Funding for open access charge: Universidad Autónoma de Barcelona.
Conflict of interest statement. None declared.

REFERENCES

1. Zlatanova,J., Caiafa,P. and Van Holde,K. (2000) Linker histone binding and displacement: versatile mechanism for transcriptional regulation. *FASEB J.*, **14**, 1697–1704.
2. Travers,A. (1999). The location of the linker histone on the nucleosome. *Trends Biochem. Sci.*, **24**, 4–7.
3. Talbert,P.B., Ahmad,K., Almouzni,G., Ausió,J., Berger,F., Bhalla,P.L., Bonner,W.M., Cande,W.Z., Chadwick,B.P., Chan,S.W. *et al.* (2012) A unified phylogeny-based nomenclature for histone variants. *Epigenetics Chromatin*, **5**, 7.
4. Shannon,M.F. and Wells,J.R (1987) Characterization of the six chicken histone H1 proteins and alignment with their respective genes. *J. Biol. Chem.*, **262**, 9664–9668.
5. Coles,L.S., Robins,A.J., Madley,L.K. and Wells,J.R. (1987) Characterization of the chicken histone H1 gene complement. Generation of a complete set of vertebrate H1 protein sequences. *J. Biol. Chem.*, **262**, 9656–9663.
6. Bates,D.L. and Thomas,J.O. (1981) Histones H1 and H5: one or two molecules per nucleosome? *Nucleic Acids Res.*, **9**, 5883–5894.
7. Sung,M.T. and Freedlender,E.F. (1978) Sites of in vivo phosphorylation of histone H5. *Biochemistry*, **17**, 1884–1890.
8. Thomas,J.O. and Rees,C. (1983) Exchange of histones H1 and H5 between chromatin fragments. A preference of H5 for higher-order structures. *Eur. J. Biochem.*, **134**, 109–115.
9. Koutzamani,E., Loborg,H., Sarg,B., Lindner,H. and Rundquist,I. (2002) Linker histone subtype composition and affinity for chromatin in situ in nucleated mature erythrocytes. *J. Biol. Chem.*, **277**, 44688–44694.
10. Orrego,M., Ponte,I., Roque,A., Buschati,N., Mora,X. and Suau,P. (2007) Differential affinity of mammalian histone H1 somatic subtypes for DNA and chromatin. *BMC Biol.*, **5**, 22.
11. Hartman,P.G., Chapman,G.E., Moss,T. and Bradbury,E.M. (1977) Studies on the role and mode of operation of the very-lysine-rich histone H1 in eukaryote chromatin. The three structural regions of the histone H1 molecule. *Eur. J. Biochem.*, **77**, 45–51.
12. Ponte,I., Vidal-Taboada,J.M. and Suau,P. (1998) Evolution of the vertebrate H1 histone class: evidence for the functional differentiation of the subtypes. *Mol. Biol. Evol.*, **15**, 702–708.
13. Vila,R., Ponte,I., Collado,M., Arrondo,J.L., Jiménez,M.A., Rico,M. and Suau,P. (2001) DNA-induced alpha-helical structure in the NH2-terminal domain of histone H1. *J. Biol. Chem.*, **276**, 46429–46435.

14. Roque,A., Iloro,I., Ponte,I., Arrondo,J.L. and Suau,P. (2005) DNA-induced secondary structure of the carboxyl-terminal domain of histone H1. *J. Biol. Chem.*, **280**, 32141–32147.
15. Lu,X. and Hansen,J.C. (2003) Revisiting the structure and functions of the linker histone C-terminal tail domain. *Biochem. Cell Biol.*, **81**, 173–176.
16. Talasz,H., Helliger,W., Puschendorf,B. and Lindner,H. (1996) In vivo phosphorylation of histone H1 variants during the cell cycle. *Biochemistry*, **35**, 1761–1767.
17. Bradbury,E.M. (1992) Reversible histone modifications and the chromosome cell cycle. *Bioessays*, **14**, 9–16.
18. Sarg,B., Helliger,W., Talasz,H., Förg,B. and Lindner,H. (2006) Histone H1 phosphorylation occurs site-specifically during interphase and mitosis: identification of a novel phosphorylation site on histone H1. *J. Biol. Chem.*, **281**, 6573–6580.
19. Roque,A., Ponte,I., Arrondo,J.L. and Suau,P. (2008) Phosphorylation of the carboxy-terminal domain of histone H1: effects on secondary structure and DNA condensation. *Nucleic Acids Res.*, **36**, 4719–4726.
20. Kaplan,L.J., Bauer,R., Morrison,E., Langan,T.A. and Fasman,G.D. (1984) The structure of chromatin reconstituted with phosphorylated H1. Circular dichroism and thermal denaturation studies. *J. Biol. Chem.*, **259**, 8777–8785.
21. Roth,S.Y. and Allis,C.D. (1992) Chromatin condensation: does histone H1 dephosphorylation play a role? *Trends Biochem. Sci.*, **17**, 93–98.
22. Gréen,A., Sarg,B., Gréen,H., Lönn,A., Lindner,H. and Rundquist,I. (2011) Histone H1 interphase phosphorylation becomes largely established in G1 or early S phase and differs in G1 between T-lymphoblastoid cells and normal T cells. *Epigenetics Chromatin*, **4**, 15.
23. Talasz,H., Sarg,B. and Lindner,H. (2009) Site-specifically phosphorylated forms of H1.5 and H1.2 localized at distinct regions of the nucleus are related to different processes during the cell cycle. *Chromosoma*, **118**, 693–709.
24. Zheng,Y., John,S., Pesavento,J.J., Schultz-Norton,J.R., Schiltz,R.L., Baek,S., Nardulli,A.M., Hager,G.L., Kelleher,N.L. and Mizzen,C.A. (2010) Histone H1 phosphorylation is associated with transcription by RNA polymerases I and II. *J. Cell Biol.*, **189**, 407–415.
25. Sarg,B., Chwatal,S., Talasz,H. and Lindner,H. (2009) Testis-specific linker histone H1t is multiply phosphorylated during spermatogenesis. Identification of phosphorylation sites. *J. Biol. Chem.*, **284**, 3610–3618.
26. Kostova,N.N., Srebreva,L., Markov,D.V., Sarg,B., Lindner,H. and Rundquist,I. (2013) Histone H5-chromatin interactions in situ are strongly modulated by H5 C-terminal phosphorylation. *Cytometry A*, **83**, 273–279.
27. Herrera,R.E., Chen,F. and Weinberg,R.A. (1996) Increased histone H1 phosphorylation and relaxed chromatin structure in Rb-deficient fibroblasts. *Proc. Natl. Acad. Sci. U.S.A.*, **93**, 11510–11515.
28. Schwarz,P.M. and Hansen,J.C. (1994) Formation and stability of higher order chromatin structures. Contributions of the histone octamer. *J. Biol. Chem.*, **269**, 16284–16289.
29. Sarg,B., López,R., Lindner,H., Ponte,I., Suau,P. and Roque,A. (2015) Identification of novel post-translational modifications in linker histones from chicken erythrocytes. *J. Proteomics*, **113**, 162–177.
30. Lindner,H., Sarg,B. and Helliger,W. (1997) Application of hydrophilic-interaction liquid chromatography to the separation of phosphorylated H1 histones. *J. Chromatogr. A*, **782**, 55–62.
31. Arrondo,J.L. and Goñi,F.M. (1999) Structure and dynamics of membrane proteins as studied by infrared spectroscopy. *Prog. Biophys. Mol. Biol.*, **72**, 367–405.
32. Lindner,H. (2008) Analysis of histones, histone variants, and their post-translationally modified forms. *Electrophoresis*, **29**, 2516–2532.
33. Lindner,H., Helliger,W., Sarg,B. and Meraner,C. (1995) Effect of buffer composition on the migration order and separation of histone H1 subtypes. *Electrophoresis*, **16**, 604–610.
34. Roque,A., Teruel,N., López,R., Ponte,I. and Suau,P. (2012) Contribution of hydrophobic interactions to the folding and fibrillation of histone H1 and its carboxy-terminal domain. *J. Struct. Biol.*, **180**, 101–109.
35. Susi,H. and Byler,D.M. (1986) Resolution-enhanced Fourier transform infrared spectroscopy of enzymes. *Methods Enzymol.*, **130**, 290–311.
36. Arrondo,J.L., Muga,A., Castresana,J. and Goñi,F.M. (1993) Quantitative studies of the structure of proteins in solution by Fourier-transform infrared spectroscopy. *Prog. Biophys. Mol. Biol.*, **59**, 23–56.
37. Noll,H. and Noll,M. (1989) Sucrose gradient techniques and applications to nucleosome structure. *Methods Enzymol.*, **170**, 55–116.
38. Roque,A., Ponte,I. and Suau,P. (2009) Role of charge neutralization in the folding of the carboxy-terminal domain of histone H1. *J. Phys. Chem. B*, **113**, 12061–12066.
39. Allan,J., Mitchell,T., Harborne,N., Bohm,L. and Crane-Robinson,C. (1986) Roles of H1 domains in determining higher order chromatin structure and H1 location. *J. Mol. Biol.*, **187**, 591–601.
40. Hendzel,M.J., Lever,M.A., Crawford,E. and Th'ng,J.P. (2004) The C-terminal domain is the primary determinant of histone H1 binding to chromatin in vivo. *J. Biol. Chem.*, **279**, 20028–20034.
41. Lu,X. and Hansen,J.C. (2004) Identification of specific functional subdomains within the linker histone H10 C-terminal domain. *J. Biol. Chem.*, **279**, 8701–8707.
42. Luque,A., Collepardo-Guevara,R., Grigoryev,S. and Schlick,T. (2014) Dynamic condensation of linker histone C-terminal domain regulates chromatin structure. *Nucleic Acids Res.*, **42**, 7553–7560.
43. Gilbert,N. and Allan,J. (2001) Distinctive higher-order chromatin structure at mammalian centromeres. *Proc. Natl. Acad. Sci. U.S.A.*, **98**, 11949–11954.
44. Ghirlando,R., Litt,M.D., Prioleau,M.N., Recillas-Targa,F. and Felsenfeld,G. (2004) Physical properties of a genomic condensed chromatin fragment. *J. Mol. Biol.*, **336**, 597–605.
45. Rodríguez-Campos,A. and Azorín,F. (2007) RNA is an integral component of chromatin that contributes to its structural organization. *PLoS One*, **2**, e1182.
46. Noll,M. and Kornberg,R.D. (1977) Action of micrococcal nuclease on chromatin and the location of histone H1. *J. Mol. Biol.*, **109**, 393–404.
47. Delcuve,G.P. and Davie,J.R. (1989) Chromatin structure of erythroid-specific genes of immature and mature chicken erythrocytes. *Biochem. J.*, **263**, 179–186.
48. Lever,M.A., Th'ng,J.P., Sun,X. and Hendzel,M.J. (2000) Rapid exchange of histone H1.1 on chromatin in living human cells. *Nature*, **408**, 873–876.
49. Contreras,A., Hale,T.K., Stenoien,D.L., Rosen,J.M., Mancini,M.A. and Herrera,R.E. (2003) The dynamic mobility of histone H1 is regulated by cyclin/CDK phosphorylation. *Mol. Cell. Biol.*, **23**, 8626–8636.
50. Kan,P.Y., Lu,X., Hansen,J.C. and Hayes,J.J. (2007) The H3 tail domain participates in multiple interactions during folding and self-association of nucleosome arrays. *Mol. Cell. Biol.* **27**, 2084–2091.
51. Hizume,K., Nakai,T., Araki,S., Prieto,E., Yoshikawa,K. and Takeyasu,K. (2009) Removal of histone tails from nucleosome dissects the physical mechanisms of salt-induced aggregation, linker histone H1-induced compaction, and 30-nm fiber formation of the nucleosome array. *Ultramicroscopy*, **109**, 868–873.
52. Stavreva,D.A. and McNally,J.G. (2006) Role of H1 phosphorylation in rapid GR exchange and function at the MMTV promoter. *Histochem. Cell Biol.*, **125**, 83–89.